AJNR

Pathology of the membranous labyrinth: comparison of T1- and T2-weighted and gadolinium-enhanced spin-echo and 3DFT-CISS imaging.

J W Casselman, R Kuhweide, W Ampe, L Meeus and L Steyaert

AJNR Am J Neuroradiol 1993, 14 (1) 59-69
http://www.ajnr.org/content/14/1/59

Pathology of the Membranous Labyrinth: Comparison of T1- and T2-Weighted and Gadolinium-Enhanced Spin-Echo and 3DFT-CISS Imaging

Jan W. Casselman,[1, 3] Rudolf Kuhweide,[2] Willy Ampe,[2] Ludo Meeus,[1] and Luc Steyaert[1]

PURPOSE: To assess the value of unenhanced T1-weighted images, T2-weighted images, gadolinium-enhanced T1-weighted images, and three-dimensional Fourier transformation-constructive interference in steady state (3DFT-CISS) images in depicting lesions of the membranous labyrinth. **METHODS:** Six patients were studied using 1-T MR; both enhanced (gadolinium-tetraazacyclododecane tetraacetic acid) and unenhanced images were obtained and different sequences compared to determine which provided the most information. **RESULTS:** A combination of gadolinium-enhanced T1-weighted and 3DFT-CISS images could depict all membranous labyrinth pathology. Unenhanced T1-weighted images were necessary to exclude spontaneous hyperintensity in the membranous labyrinth. Gadolinium-enhanced T1-weighted images were needed to detect enhancing pathology such as labyrinthitis and tumors inside the membranous labyrinth. In these cases, 3DFT-CISS images allowed immediate differentiation between inflammation and tumor. In temporal bone tumors involving the bony and membranous labyrinth, unenhanced and enhanced T1-weighted images often sufficed to suggest the correct diagnosis. Only 3DFT-CISS images were able to demonstrate small structures (as fistulas) and to help us confirm or rule out obliteration of the labyrinthine fluid spaces. 3DFT-CISS images were necessary to detect small congenital malformations of the membranous labyrinth when only MR was performed. Uncalcified obliteration of the labyrinth fluid spaces could be reliably detected only on 3DFT-CISS images. Here also gadolinium-enhanced T1-weighted images had to be obtained because enhancement of the soft tissues inside the membranous labyrinth had been observed. **CONCLUSION:** The CISS sequence and enhanced T1-weighted sequence formed the best sequence combination for diagnosis of membranous labyrinth lesions; additional, unenhanced T1-weighted images can help one differentiate labyrinthitis, proteinaceous fluid, subacute hemorrhage, or tumor inside the labyrinth.

Index terms: Temporal bone, magnetic resonance; Contrast media, paramagnetic; Magnetic resonance, technique

AJNR 14:59–69, Jan/Feb 1993

Initially, the radiologic study of the temporal bony labyrinth was restricted to conventional radiographic studies, later improved with polytomographic techniques. With the advent of computed tomography (CT), it became possible to detect soft-tissue lesions in the cerebellopontine angle and internal acoustic canal (IAC) and more detailed study of the bony labyrinth became possible. Recently magnetic resonance (MR) emerged as an excellent diagnostic method in the diagnosis of membranous labyrinth lesions. First only routine T1- and T2-weighted spin-echo sequences were used, showing normal anatomy, congenital lesions, and relatively large tumors of the membranous labyrinth (1). The application of gadolinium (Gd) was a major step forward and diagnosis of small intralabyrinthine tumors (schwannomas, extension of metastases along cranial nerves) and inflammatory lesions (labyrinthitis) became possible (2, 3). Finally, three-dimensional Fourier transform (3DFT) imaging made detailed anatomic studies (4, 5) of the membranous labyrinth possible and also had the potential to add new

Received October 25, 1991; revision requested February 7, 1992; revision received May 6 and accepted July 20.

From the [1]Department of Radiology, and [2]Otorhinolaryngology, A. Z. St.-Jan Brugge, Brugge, Belgium.

[3] Address reprint requests to J. W. Casselman, Department of Radiology, A. Z. St.-Jan Brugge, Ruddershove 10, B-8000 Brugge, Belgium.

AJNR 14:59–69, Jan/Feb 1993 0195-6108/93/1401-0059

information to a routine spin-echo study of the pathologic membranous labyrinth (5, 6). The possibility of making multiplanar and 3-D reconstructions from a 3DFT data set certainly facilitated labyrinth examination (5, 6).

Six patients presenting with sensorineural hearing loss (SNHL) or vestibular dysfunction and who eventually had membranous labyrinth lesions were selected from a group of patients presenting with the same symptoms. All in the group were screened for acoustic schwannomas with unenhanced and enhanced T1-weighted images, T2-weighted images, and 3DFT-constructive interference in steady state (CISS) images. In the six patients selected, the different sequences were compared to find out which single sequence or pair of sequences provided optimal information.

Subjects and Methods

Six patients (average age, 24 years; three women and three men) presenting with SNHL or vestibular dysfunction and who eventually had a membranous labyrinth lesion were studied. Clinical examination included audiometry and electronystagmographic vestibular examination (including both caloric and rotational chair tests). Patients with SNHL or vestibular dysfunction and a lesion only present in the IAC or patients with lesions along the facial nerve were excluded from the study. Pathology included labyrinthitis, intravestibular schwannoma, cholesterol granuloma with fistula towards the labyrinth, fibrous dysplasia with labyrinth involvement, large vestibular aqueduct syndrome, and Cogan syndrome.

All patients underwent MR on a 1.0-T superconductive active shielded magnet including 3-mm contiguous axial unenhanced and Gd-tetra-azacyclododecane tetraacetic acid-enhanced (Dotarem, Guerbet Laboratories, Aulnay-sous-Bois, France) T1-weighted 2–D spin-echo images, 500/15/4 (TR/TE/excitations), 4-mm axial T2-weighted 2-D spin-echo images, 2500/15, 90/1 with a 0.8-mm gap, and 1-mm contiguous axial 3DFT-CISS images. The total acquisition time was 8 minutes 32 seconds for the T1- and 10 minutes 40 seconds for the T2-weighted images. All images were obtained using a circular polarized head coil. In each patient, the value of T1-, T2-, and Gd-enhanced T1-weighted images and CISS images were evaluated.

The following scoring system was applied: (−) = pathology not detected with this sequence or sequence pair alone, (+) = diagnosis possible, additional information provided by other sequences required, (++) = complete diagnosis can be made with this sequence or sequence pair alone. In each case the sequence or sequence pair providing the most adequate information was indicated by "*".

The CISS sequence scheme, providing the CISS images, is a 3DFT sequence scheme using the steady-state free precession of spins (Deimling M et al, paper presented at the annual meeting of the Society for Magnetic Resonance in Medicine, Amsterdam, August 1989). In this sequence scheme a "true" fast imaging with steady precession (FISP) sequence is run once with alternating and once with nonalternating radiofrequency pulses. This sequence scheme was already described in more detail (see companion article) (5). In the CISS sequence scheme, flow compensation techniques are used to make sure that spins, independent of their actual velocity, are being refocused. The flow compensation is applied to each gradient over each repetition time (TR) cycle, unlike standard flow compensation sequences (eg, motion refocusing angiography sequences) in which the flow compensation is applied to the echo. All three gradients are balanced, indicating that the average value of each gradient is zero. In this case, spins moving at a constant velocity will have the same phase after the application of the gradient pulses that they had before (7), resulting in high signal of all cerebrospinal fluid and labyrinthine fluid (endolymph/perilymph) spaces.

Such a steady-state flow-compensated 3D-FISP sequence with symmetrical gradients will produce images that show bands of low signal intensity. These dark bands are caused by small magnetic field inhomogenities and local field distortions due to susceptibility changes that are normally produced by the patient. The solution to this problem is to acquire two data sets successively with a true FISP sequence of alternating and nonalternating radiofrequency pulses (5). A mathematical postprocessing operation (maximum intensity projection (MIP)) takes the information of each pair of images of the two 3-D data sets created in this way to produce an image with a homogeneous intensity distribution over the whole image. Used parameters are 1 slab of 32-mm thickness, 32 partitions, TR = 20 msec, echo time (TE) = 8 msec, matrix = 256 × 256, field of view = 176 mm; the result is 1-mm sections with an in-plane resolution of 0.69 × 0.69 mm and a total acquisition time of 2 times 2 minutes 46 seconds. In four patients (cases 2, 4, 5, and 6) 3-D reconstructions of the membranous labyrinth were made by applying a targeted MIP on the 3DFT-CISS images.

Results

All clinical and MR findings are presented in Table 1. The diagnostic value of all single sequences and sequence pairs are evaluated in Table 2. Clinical audiologic and vestibular signs correlated well with the anatomical localization and side where the pathology was found in all cases.

On T1- and T2-weighted images, a complete diagnosis was possible in three and two cases, respectively. Gd-enhanced T1-weighted images detected pathology in five cases, but additional information provided by other sequences was necessary to make the exact diagnosis in three cases. When a combination of unenhanced and Gd-enhanced T1-weighted images was used, then

TABLE 1: Clinical and MR data on patients with membranous labyrinth pathology

Case	Age/Sex	Diagnosis/Affected Side	Clinical Presentation (Audiologic/Vestibular)	MR Findings		
				T1/T2	T1-Gd	CISS
1	46/M	Labyrinthitis/R	Sudden deafness/vestibular areflexia	Normal	Enhancement of C, V, ampullae of LSC, PSC and SSC	Normal
2	17/F	Schwannoma in vestibulum/L	SNHL/spontaneous nystagmus to the right, pathologic rotational and caloric tests	2-mm isointensity[a] lesion in V/signal loss in V	Enhancement in V and ampulla of PSC	Filling defect in V
3	46/F	Cholesterol granuloma fistula to PSC/L	SNHL in the low-frequency range/vestibular areflexia	High-intensity[a] lesion posterior of porus and in V and PSC	Same findings, no enhancement	Visualization of fistula
4	15/F	Fibrous dysplasia with labyrinth involvement/R	Slight SNHL in the low-frequency range/ vestibular areflexia	Hypointense[a] abnormal bone and LSC, PSC, SSC destruction + EAC narrowing/ isointense[a] bone	Weak enhancement of bone, destruction LSC, PSC, SSC	Obliteration of semicircular canals
5	14/M	Large vestibular aqueduct syndrome/R	Progressive SNHL, mainly in the high-frequency range	Enlarged VA	Enlarged VA	Enlarged VA
6	22/M	Cogan syndrome	Bilateral subtotal SNHL/ bilateral vestibular areflexia interstitial keratitis	Normal	Normal	Narrowing of PSC and SSC

Note.—Abbreviations: C = cochlea, EAC = external auditory canal, LSC = lateral semicircular canal, PSC = posterior semicircular canal, SSC = superior semicircular canal, V = vestibulum, VA = vestibular aqueduct, SNHL = sensorioneural hearing loss.

[a] Hyper-, iso- or hypointense compared to brain tissue.

TABLE 2: Value of different sequences in patients with membranous labyrinth pathology

Case	Diagnosis	T1	T2	T1-Gd	CISS	T1 + T2	T1 + T1-Gd	T1 + CISS	T2 + T1-Gd	T2 + CISS	T1-Gd + CISS
1	Labyrinthitis	−	−	+	−	−	++*	−	+	−	+
2	Ultriculosaccular schwannoma	++	−	+	+	++	++*	++	+	+	++
3	Cholesterol granuloma with fistula to PSC	+	+	+	+	++*	+	+	+	+	+
4	Fibrous dysplasia with labyrinth destruction	++	++	++	+	++	++	++	++	++	++*
5	Large vestibular aqueduct syndrome	++	++	++	++*	++	++	++	++	++	++
6	Cogan syndrome	−	−	−	+*	−	−	+	−	+	+

Note.—(−) = diagnosis not possible with this single sequence or pair of sequences; (+) = pathology was recognized, additional information provided by other sequences required to make exact diagnosis; (++) = diagnosis can be made with this single sequence or pair of sequences alone; (*) = optimal single sequence or pair of sequences in this case; PSC = posterior semicircular canal.

pathology was detected in five cases and an exact diagnosis was possible in four of the six cases. In one case (case 3), the final diagnosis was made when both unenhanced T1- and T2-weighted images were used. The CISS sequence provided important additional information in four cases, also resulting in the best single sequence in cases 5 and 6 and best sequence pair in case 4. A combination of CISS images and Gd-enhanced T1-weighted images was necessary to detect the pathology in all cases and also made an exact diagnosis possible in three of the six cases.

Discussion

More lesions of the labyrinth are being diagnosed since the introduction of MR, especially with Gd-enhanced and 3DFT imaging techniques (2–6). A good choice of sequences is necessary to detect the lesion and make the correct diagnosis. These sequences should also be used when one is screening for acoustic schwannomas. An acoustic schwannoma is often difficult to differentiate from a labyrinthine lesion on a clinical basis (3); therefore, screening sequences must be selected so that a maximum of labyrinthine lesions can be detected in case no IAC or cerebellopontine angle schwannomas are found. Our study shows that the Gd-enhanced T1-weighted sequence is very sensitive; however, uncalcified obliteration of the intralabyrinthine fluid spaces is recognized only on CISS images. The value of the different sequences depends on the pathology one is dealing with. In our study, the combination of a Gd-enhanced T1-weighted sequence and a CISS sequence scheme resulted in the highest sensitivity (Table 2).

Pathology Causing Contrast Enhancement Inside the Membranous Labyrinth

Localized enhancement in the labyrinth in cases of inflammation (case 1) (Fig. 1) and of tumors (case 2) (Fig. 2) has been described (2, 3, 8). It is caused by breakdown of the blood-brain/labyrinth barrier (9, 10) and explains the high sensitivity of the Gd-enhanced T1-weighted sequence. In case of inflammation (viral and luetic labyrinthitis), Gd accumulation in the affected membranous labyrinth and its endolymphatic content probably causes the enhancement. In these cases, often more than one part (cochlea-vestibule-semicircular canals) of the labyrinth enhances and the edges of the enhancement are not sharp (Fig. 1). These signs can be used in the differential diagnosis between inflammatory and tumoral enhancement of the membranous labyrinth. When a tumor is present inside the membranous labyrinth, the contrast enhancement is more likely restricted to one part of the membranous labyrinth and the edges of the enhancing lesion are sharp (Fig. 2B), although it can still be difficult to differentiate between inflammation and tumor even when both clinical information and the Gd-enhancement pattern are known. In these cases, follow-up studies have been used to make differentiation possible. In case of labyrinthitis, the enhancement disappears after some months, while in case of tumor the enhancement persists. Immediate differentiation is now possible when 3DFT-CISS images are available. In case of labyrinthitis, Gd accumulation inside the membranous labyrinth will not be recognized on the CISS images and normal labyrinthine fluid spaces will be seen. But when a tumor is present, the tumor mass will replace the endolymph and loss of high signal can be seen (Fig. 2). It can, however, be difficult to decide whether one is dealing with a lesion or a volume-averaging artifact when such a signal loss is seen on a 1-mm axial section. In these cases, the 3-D labyrinth reconstructions play an important role. Volume-averaging artifacts can be excluded when 3-D membranous labyrinth reconstructions are made (Figs. 2C–2D) and pathology is more easily recognized when the 3-D reconstructions of both sides are compared.

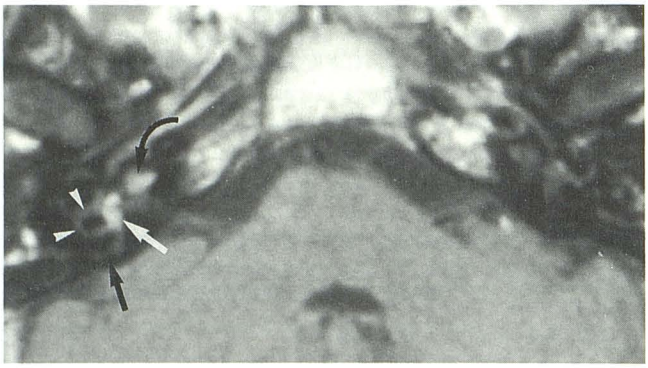

Fig. 1. Presumed viral labyrinthitis (case 1). Axial Gd-enhanced T1-weighted image (500/15/4) through both inner ears. Marked enhancement is seen in the right cochlea (*curved black arrow*), utriculosaccular structures (*large white arrow*), posterior (*large black arrow*), and lateral semicircular canal (*white arrowheads*). Normal intensities are seen in the left cochlea and labyrinth.

Spontaneous high signal inside the labyrinth on T1-weighted images is theoretically possible in case of subacute hemorrhage in the labyrinth and when a high protein level is present inside the fluid spaces (elevated protein in perilymphatic fluid has been reported in patients with acoustic schwannomas). Therefore, it is necessary to start the study with an unenhanced T1-weighted sequence in order to differentiate enhancement from spontaneous hyperintensity. The value of CT in case of labyrinthitis and intralabyrinthine tumors is limited; in cases 1 and 2, the pathology was not recognized on CT. CT can detect only the end stage of labyrinthitis: "labyrinthine ossification."

In conclusion, unenhanced and enhanced T1-weighted images in combination with CISS im-

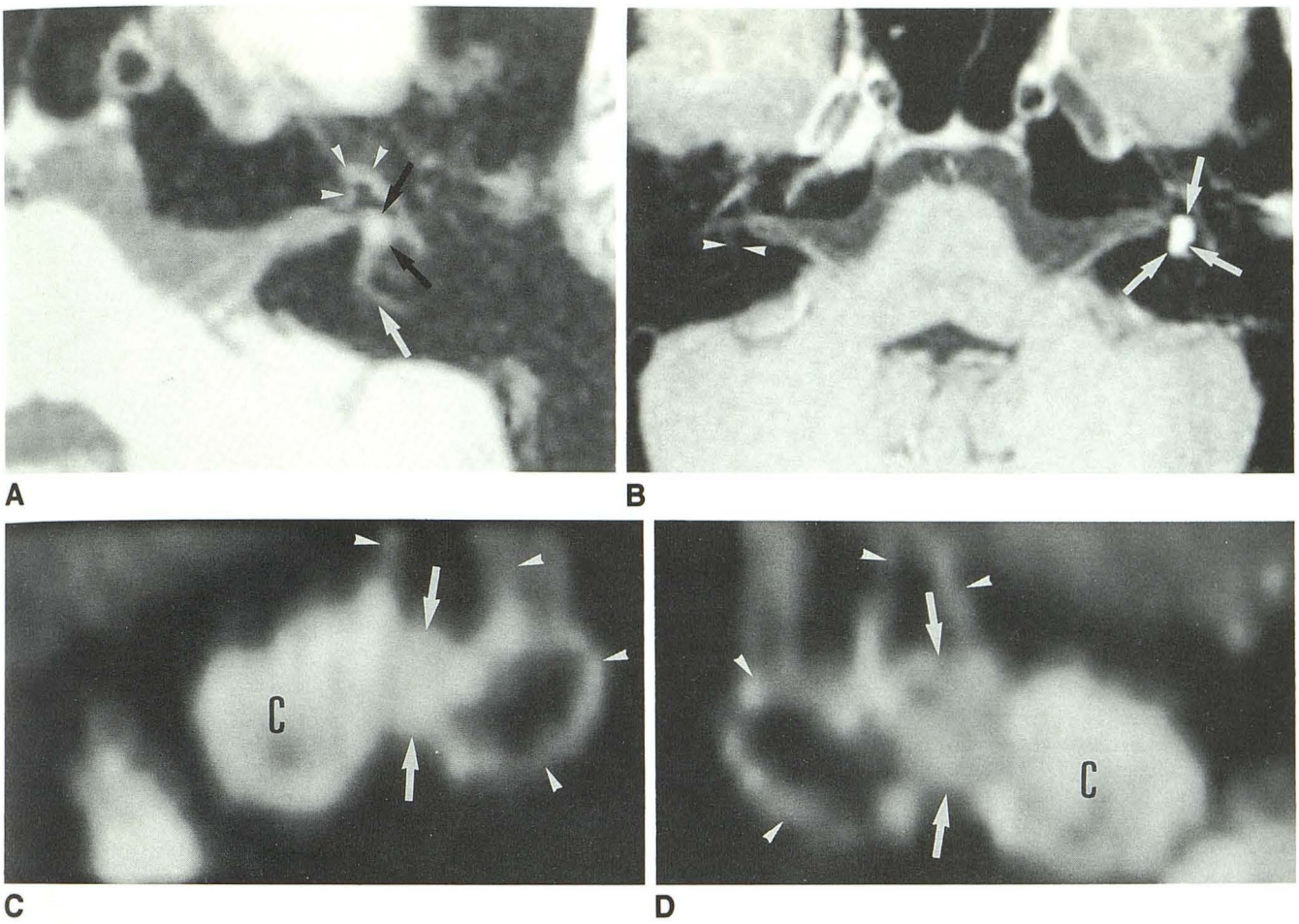

Fig. 2. Utriculosaccular schwannoma.

A, Axial unenhanced T1-weighted image (500/15/4) through the left membranous labyrinth. Appropriate windowing makes a small lesion in the utriculosaccular structures visible as a 1.5-mm hyperintense lesion (*large black arrows*). Posterior semicircular canal (*large white arrow*), anterior segment, geniculate ganglion, and horizontal segment of the facial nerve (*white arrowheads*).

B, Gd-enhanced axial T1-weighted image (500/15/4) through both inner ears. Marked enhancement is seen throughout the left utriculosaccular structures in a larger area than could be expected on the unenhanced images (*large white arrows*). Compare with the normal low signal in these structures on the right (*white arrowheads*).

C and *D*, 3-D MIP reconstructions (from CISS images) of the right (*C*) and left (*D*) cochlea and labyrinth. Normal high signal intensity in cochlea (*C*), utriculosaccular structures (*large white arrows*), and semicircular canals (*white arrowheads*) on the right (*C*). On the left side (*D*) the endolymph is replaced by a tumoral mass inside the utriculosaccular structures, resulting in lower signal (*large white arrows*). Semicircular canals (*white arrowheads*), cochlea (*C*).

ages are able to show the above-mentioned pathology and lead to the correct diagnosis. T2 and CISS images alone cannot be used as screening sequences because they do not show labyrinth inflammation.

Temporal Bone Tumors Involving the Bony and Membranous Labyrinth

Benign and malignant tumoral lesions can cause destruction of the bony labyrinth and can also obliterate the labyrinthine fluid spaces (cases 3 and 4). Unenhanced and Gd-enhanced T1-weighted images and T2-weighted images all contribute to the tissue characterization of the lesions. T2-weighted images, however, are not always necessary. In case 3 (surgically confirmed cholesterol granuloma), the T2-weighted images allowed further differentiation between a cholesterol granuloma and a congenital cholesteatoma. Both can present as a spontaneous high-signal lesion on T1-weighted images (Fig. 3A). In the first case, the signal remains very high (Fig. 3B), in the latter, slight fading is seen on T2-weighted images (1). But high signal on T1-weighted images in case of congenital cholesteatoma is rare; most often, signal intensities intermediate to the intensities of liquor and brain tissue are described (11). This reduces the value of T2-weighted images in this particular case. In many other lesions,

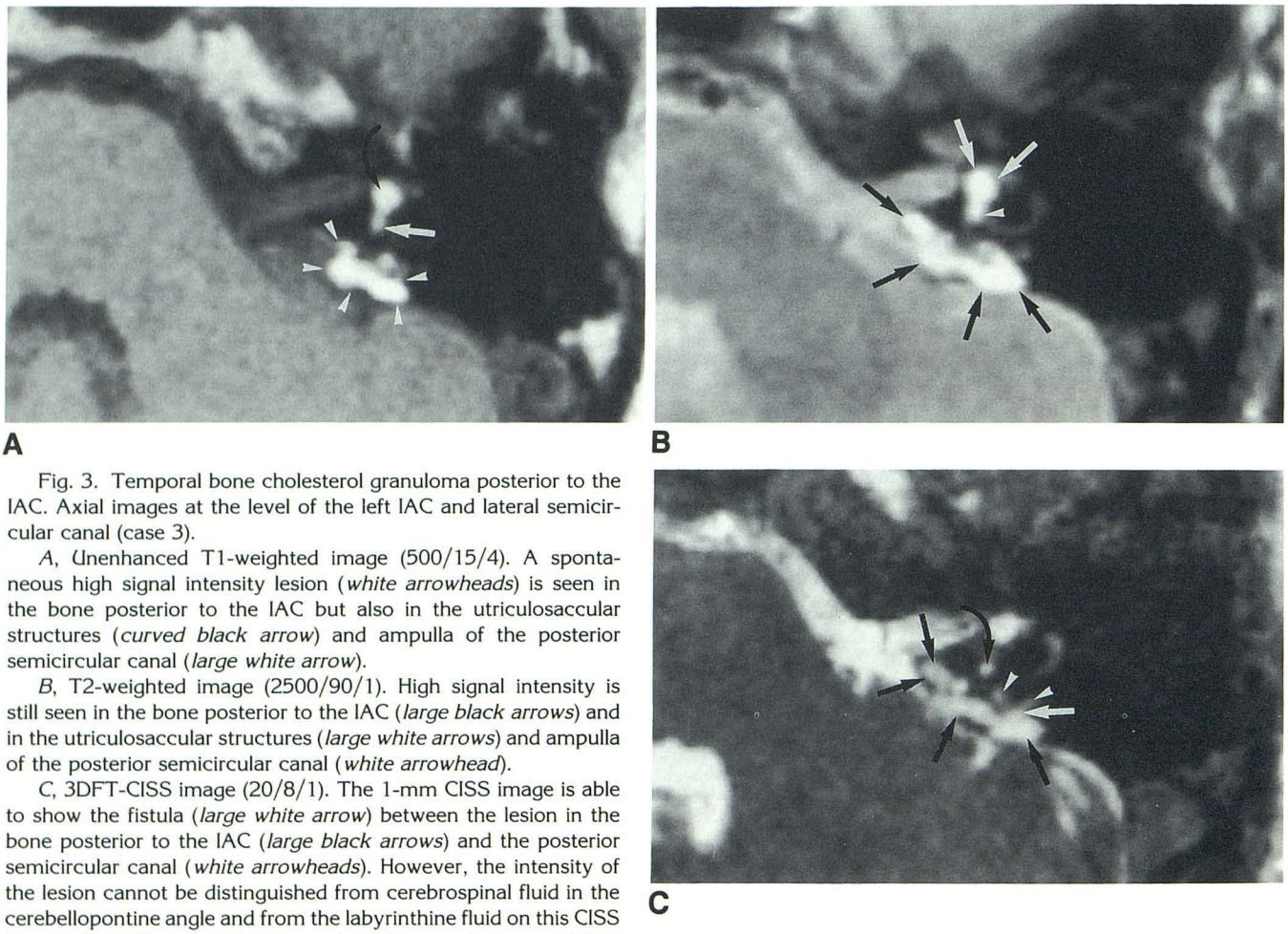

Fig. 3. Temporal bone cholesterol granuloma posterior to the IAC. Axial images at the level of the left IAC and lateral semicircular canal (case 3).

A, Unenhanced T1-weighted image (500/15/4). A spontaneous high signal intensity lesion (*white arrowheads*) is seen in the bone posterior to the IAC but also in the utriculosaccular structures (*curved black arrow*) and ampulla of the posterior semicircular canal (*large white arrow*).

B, T2-weighted image (2500/90/1). High signal intensity is still seen in the bone posterior to the IAC (*large black arrows*) and in the utriculosaccular structures (*large white arrows*) and ampulla of the posterior semicircular canal (*white arrowhead*).

C, 3DFT-CISS image (20/8/1). The 1-mm CISS image is able to show the fistula (*large white arrow*) between the lesion in the bone posterior to the IAC (*large black arrows*) and the posterior semicircular canal (*white arrowheads*). However, the intensity of the lesion cannot be distinguished from cerebrospinal fluid in the cerebellopontine angle and from the labyrinthine fluid on this CISS image. Ampulla of posterior semicircular canal (*curved black arrow*).

as in the case of fibrous dysplasia (case 4), T1-weighted images without and with Gd administration suffice to make the exact diagnosis and T2-weighted sequences are of limited value.

In contrast, additional important information is often added by 3DFT-CISS images (cases 3 and 4). Thin adjacent sections with high spatial and contrast resolution are needed to detect small lesions, such as fistulas, between tumors and the membranous labyrinth (Fig. 3C). These small lesions or structures can be missed on 3- to 4-mm T1- and T2-weighted images. 3DFT-CISS images are also required to detect obliteration of the labyrinthine fluid spaces. Obliteration is confirmed when the high signal of the labyrinthine fluid is lost. Here again oblique sections through the labyrinth structures and volume-averaging artifacts could give a false impression of obliteration on the axial thin CISS images. On 3-D reconstructions, the three semicircular canals, the cochlea, and the vestibule are always completely visible. Any interruption of these structures on the 3-D reconstructions represents obliteration of the labyrinthine fluid spaces (Figs. 4B and 4C). Consequently the Gd-enhanced T1 and CISS sequence pair turned out to be the best sequence combination in case 4 and allowed detection of the pathology in case 3.

CT was able to make the correct diagnosis in case 4 but obliteration of the fluid spaces inside the posterior and lateral semicircular canal could only be suspected. In case 3, CT allowed detection of the lesion in the bone posterior to the IAC but the exact diagnosis of cholesterol granuloma was not possible without MR. The fistula and extension of the granuloma inside the membranous labyrinth were not recognized on CT. These cases show that in case of temporal bone tumors with involvement of the bony and membranous labyrinth T1- and T2-weighted MR often surpasses CT in the characterization of the lesion, and that obliteration of the labyrinthine fluid spaces is best demonstrated on 3DFT-CISS images.

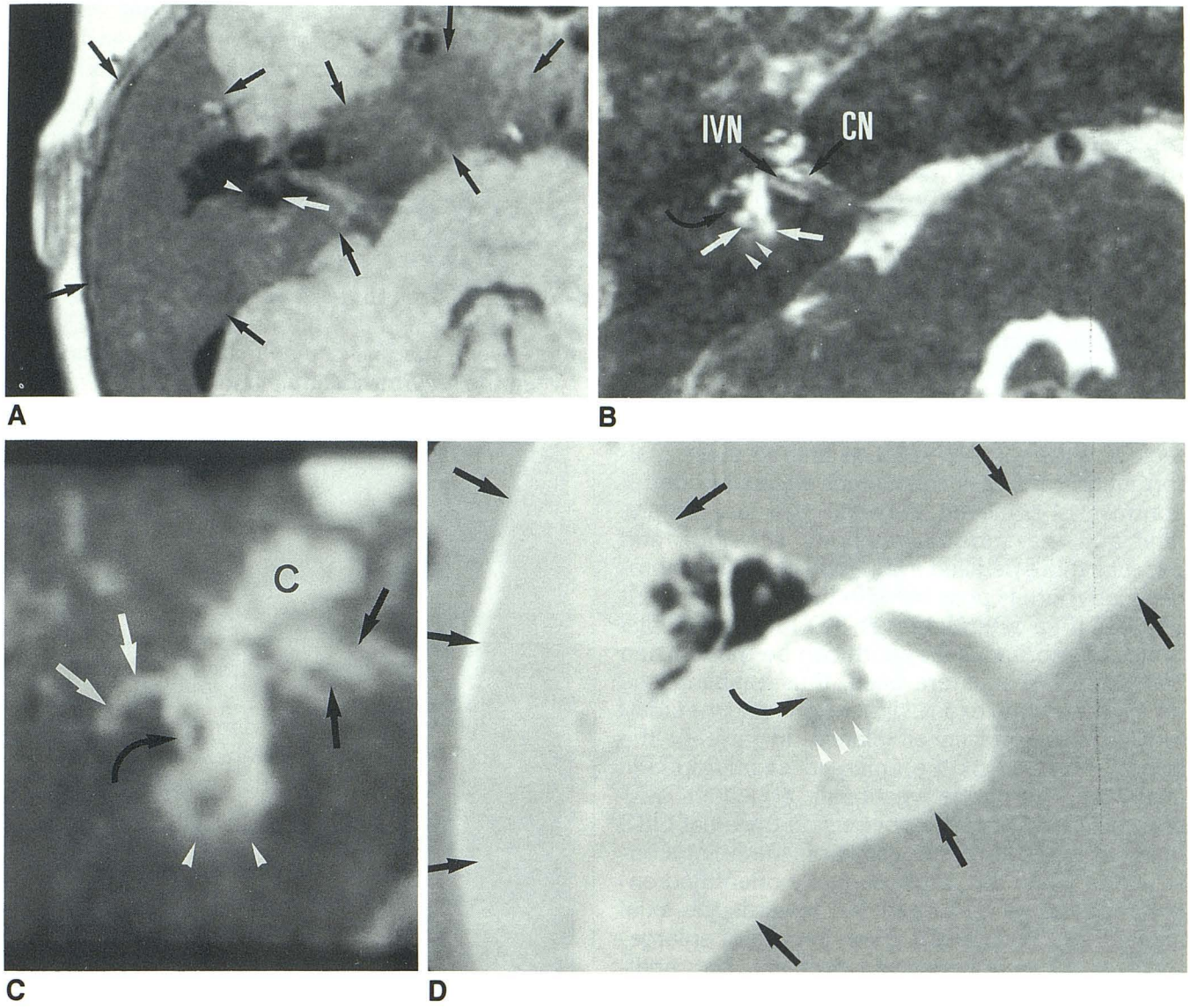

Fig. 4. Fibrous dysplasia with labyrinth involvement (case 4).

A, Axial unenhanced T1-weighted image (500/15/4) through the right inner ear. Thickening of the temporal bone and sphenoid bone (*large black arrows*) is seen. The diffuse bone alteration is hypointense compared to brain tissue and the lateral (*white arrowhead*) and posterior semicircular canal (*large white arrow*) seem to be interrupted; however, volume-averaging artifacts (3-mm sections) can make a definite diagnosis impossible.

B, Axial 1-mm 3DFT-CISS image (20/8/1) through the right inner ear. The posterior part of the fluid in the lateral semicircular canal was seen neither on this image nor on the adjacent sections (*curved black arrow*). The fluid inside the posterior semicircular canal (*white arrowheads*) was also absent, confirming obliteration of this canal. The borders of the posterior semicircular canal ampulla and of the common crus were irregular and represent partial obliteration of these structures (*large white arrows*). Cochlear nerve (*CN*), inferior vestibular nerve (*IVN*). Normally there is no involvement of the otic capsule and labyrinth structures in case of temporal bone fibrous dysplasia (12, 13). Here, involvement of the labyrinth was proven by CT and MR and the diagnosis of fibrous dysplasia was confirmed by biopsy.

C, 3-D reconstructions of the right labyrinth made by applying a targeted MIP on the 3DFT-CISS images. Only part of the fluid in the lateral (*large white arrows*) and posterior (*white arrowheads*) semicircular canal was seen, proving that there is obliteration of these structures. An impression on the superior semicircular canal is also demonstrated (*curved black arrow*). Normally these 3-D reconstructions can always be turned in space so that all three semicircular canals are visible (see also Fig. 4 in Casselman et al (5)). Cochlea (*C*), nerves inside the IAC (*large black arrows*).

Note: For corresponding drawing of this 3-D reconstruction see Figure 10C in Casselman et al (5).

D, Axial CT image through the right labyrinth. Diffuse bone alteration (*large black arrows*) is present in the temporal bone. Involvement of the posterior part of the lateral semicircular canal (*curved black arrow*) and bone alterations in the region where the posterior semicircular canal is expected (*white arrowheads*). CT proves that bone destruction is present but allows no evaluation of the exact amount of labyrinthine fluid that is still present inside the altered bony labyrinth.

Congenital Malformations of the Membranous Labyrinth

Patients with congenital malformations of the membranous and bony labyrinth frequently present with SNHL (14). Clinicians cannot always make the distinction between SNHL due to congenital labyrinth malformation and SNHL due to acoustic schwannoma, therefore, many of these patients are initially studied with MR in order to exclude or detect an acoustic schwannoma. However, when the MR technique is not adapted to this problem, small labyrinth malformations (malformations of the lateral semicircular canal, large endolymphatic duct and sac, etc) are more difficult to see (Fig. 5A) and may even remain undetected. With a 3DFT-CISS technique these malformations are easier to detect because a better contrast is achieved between the labyrinthine fluid and the surrounding bony labyrinth, and because more detailed evaluation of the membranous labyrinth is possible with the 1-mm adjacent sections (Fig. 5B). Moreover 3-D reconstructions of the membranous labyrinth can be made when 3DFT-CISS images are used, thus enabling one to evaluate the exact dimensions of the malformed structures in all planes. In case 5, the largest diameter of the enlarged endolymphatic duct and sac (large vestibular aqueduct syndrome) (14–16) are not obvious on the axial CISS image (Fig. 5B) but are visible on the 3-D reconstruction when the rather sagitally orientated endolymphatic sac is turned 30° towards the axial plane (Figs. 5C and 5D). Even in case of enlargement of the endolymphatic duct and sac, additional Gd-enhanced T1-weighted images are mandatory because Gd enhancement has been noticed inside an enlarged endolymphatic sac in patients with Meniere disease (idiopatic hydrops) (Mark AS et al, paper presented at the annual meeting of the American Society of Neuroradiology, Washington, June 1991). These malformations of the inner ear can of course be detected on CT, but, as already mentioned, these patients are often first screened with MR to exclude acoustic schwannomas. Therefore, the routine MR technique should include a 3DFT-CISS sequence to detect small congenital malformations of the labyrinth.

Pathology Causing Obliteration of the Labyrinthine Fluid Spaces

CT is able to demonstrate calcified obliteration of the labyrinthine fluid spaces (labyrinthitis ossificans). However, it is probable that calcified obliteration is the end stage of earlier and more frequent uncalcified soft tissue obliteration. This soft-tissue obliteration is not visible on CT, but can be seen on 3DFT-CISS. On these images, the normal high signal of the labyrinthine fluid is replaced by low-signal soft tissues (Fig. 6), which can also be seen when a tumor is present inside the membranous labyrinth (Fig. 2). Again, 1-mm sections are necessary to exclude obliteration of small structures, and 3-D reconstructions are very helpful to exclude volume-averaging artifacts. Moreover, images displaying high contrast between the labyrinthine fluid and surrounding bone are needed. The 3DFT-CISS images offer all these advantages and possibilities and, therefore, often detect obliteration when 3- to 4-mm T2- and unenhanced and Gd-enhanced T1-weighted images and CT are normal. We have found uncalcified soft-tissue obliteration of the labyrinthine fluid spaces (recognized only on 3DFT-CISS images) in patients with Cogan syndrome, (case 6) and otosclerosis, as well as in cochlear implant candidates who were suffering from postmeningitic deafness.

Gd-enhanced T1-weighted images remain necessary to differentiate between a rare intralabyrinthine tumor (case 2) and inflammatory soft-tissue obliteration. But differentiation can even then remain difficult, as when we recently found Gd enhancement in the obliterating soft tissues in a patient with Cogan syndrome. Cogan syndrome is a rare syndrome, occurring in young adults presenting with nonsyphilitic interstitial keratitis, vestibuloauditory dysfunction, and vasculitis. Thickening of the membranous lining of the labyrinth walls and the presence of connective tissue with a mesenchymatous appearance or acidophilic coagulae inside the labyrinth have been reported (17, 18). Gd enhancement of the membranous labyrinth in these patients probably reflects active disease with inflammation of the blood vessels of the stria vascularis.

Conclusion

The CISS sequence and the enhanced T1-weighted MR sequence (3-mm sections) formed the most sensitive sequence pair in the diagnosis of membranous labyrinth lesions. Moreover, they allow excellent screening for acoustic schwannomas and labyrinth lesions, which are difficult to differentiate clinically. An additional unenhanced T1-weighted sequence should be consid-

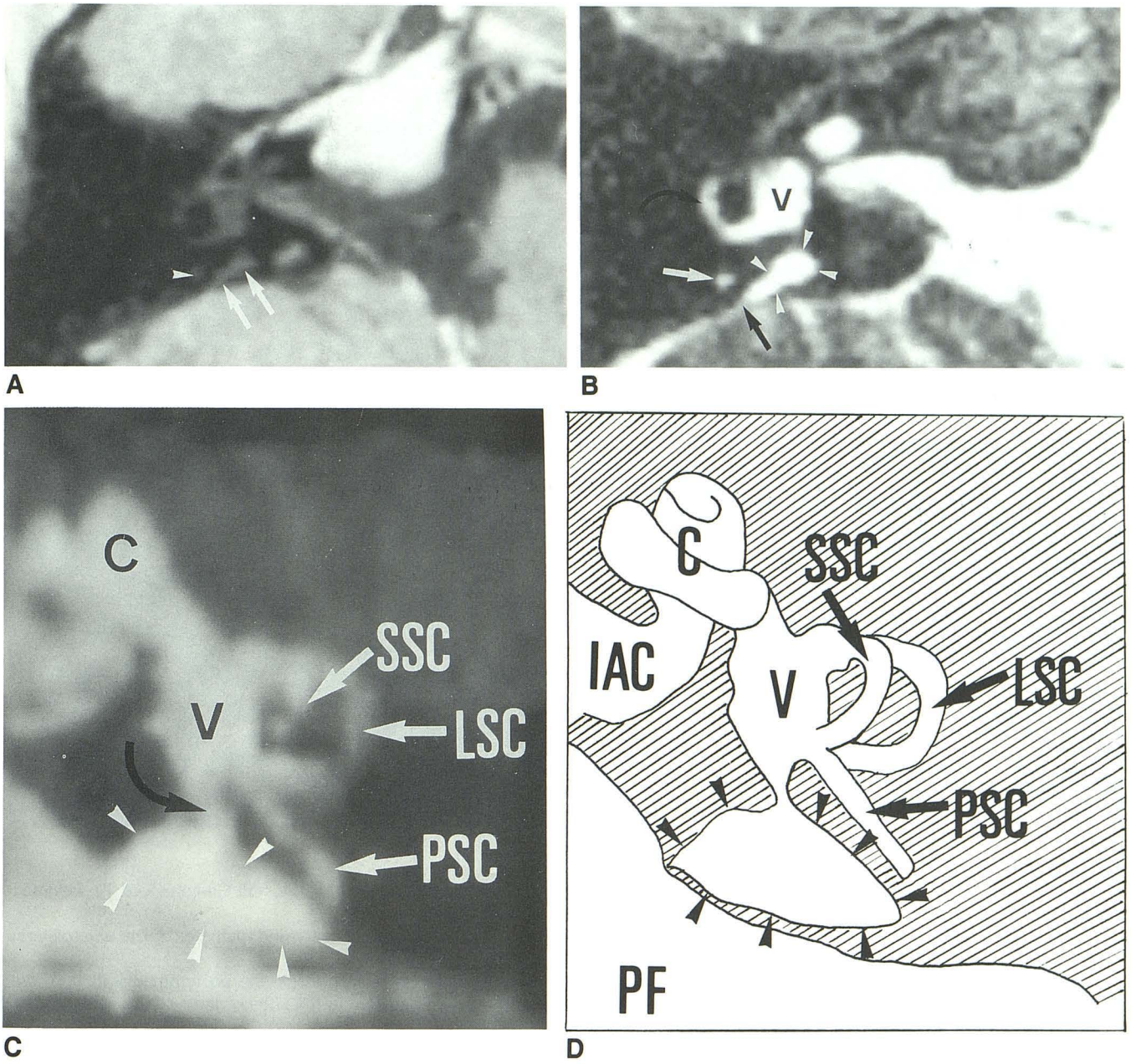

Fig. 5. Large vestibular aqueduct syndrome (case 5).

A, Axial unenhanced T1-weighted image (500/15/4) at the level of the right lateral semicircular canal. The enlarged endolymphatic sac (*large white arrows*) can be seen medial of the ascending limb of the posterior semicircular canal (*white arrowhead*).

B, Axial 1-mm CISS image (20/8/1) at the level of the right lateral semicircular canal. The enlarged vestibular aqueduct (*white arrowheads*) and its relation to the posterior semicircular canal (*large white arrow*) is better seen. The endolymphatic sac can also be seen close to the cerebrospinal fluid in the posterior fossa (*large black arrow*) but no fistula is present. Lateral semicircular canal (*curved black arrow*), vestibule (*V*).

C, 3-D reconstruction of the labyrinth made by applying a targeted MIP on the 3DFT-CISS images. This 3-D reconstruction was rotated so that the normal parasagittal-orientated vestibular aqueduct was turned 30° towards the axial plane. In this projection, the real dimension of the endolymphatic sac can be appreciated and is now seen as a plane (triangle) rather than as the linear structure that was seen on the axial image. The connection (*curved black arrow*) between the enlarged endolymphatic sac (*white arrowheads*) and the vestibulum (*V*) was recognized. Lateral semicircular canal (*LSC*), posterior semicircular (*PSC*), superior semicircular canal (*SSC*), and cochlea (*C*).

D, Drawing of the 3-D reconstruction of the labyrinth (*C*). Only 3-D membranous labyrinth reconstructions allow evaluation of the largest dimensions of the endolymphatic sac (*black arrowheads*) because these images can be rotated freely in space. Cochlea (*C*), internal auditory canal (*IAC*), lateral (*LSC*), posterior (*PSC*), and superior semicircular canal (*SSC*), vestibule (*V*), posterior fossa (*PF*).

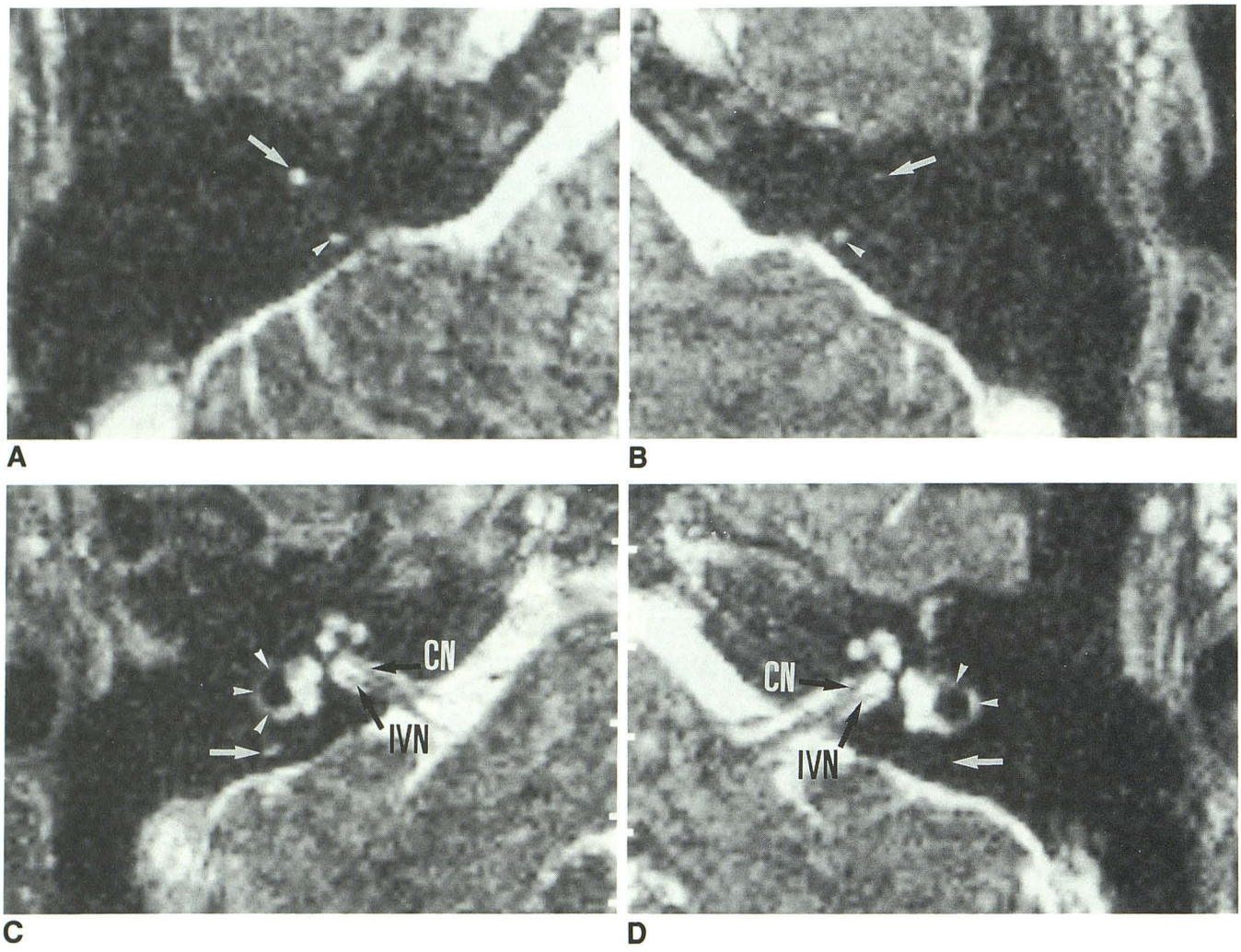

Fig. 6. Patient with Cogan syndrome (case 6). CT was normal; no pathology was seen on T1-, T2-, and Gd-enhanced T1-weighted images.

A, Axial CISS image at the level of the right superior semicircular canal. Normal signal intensity and diameter of the anterolateral (*large white arrow*) and posteromedial (*white arrowhead*) limb of the superior semicircular canal.

B, Axial CISS image at the level of the left superior semicircular canal. Endolymph is seen inside the posteromedial limb (*white arrowhead*) of the superior semicircular canal, but only very little endolymph can be detected in the anterior limb due to narrowing of the canal (*large white arrow*).

C, Axial CISS image through the right vestibule and cochlea. The endolymph inside the posterior semicircular canal can be seen (*large white arrow*). Lateral semicircular canal (*white arrowheads*), cochlear nerve (*CN*), and inferior vestibular nerve (*IVN*) (*large black arrows*).

D, Axial CISS image through the left vestibulum and cochlea. The fluid inside the posterior semicircular canal cannot be visualized (*large white arrow*) representing total or subtotal obliteration of the canal. Lateral semicircular canal (*white arrowheads*), cochlear nerve (*CN*), and inferior vestibular nerve (*IVN*) (*large black arrows*).

ered in order to differentiate labyrinthitis, proteinaceous fluid, subacute hemorrhage, or tumor inside the labyrinth.

Acknowledgments

We thank Siemens U B Med.-Erlangen for putting to our disposal the work-in-progress version of the CISS sequence scheme and we also thank Greta Vandemaele and Bavo Van Riet (MR-application, Siemens, Brussels) for adapting the CISS sequence scheme to the needs of this study and for the information they provided concerning this sequence. We also thank Dr J. Clarysse and Dr R. Loncke (Department of Otorhinolaryngology, H. Hart Hospital Roeselare, Belgium) and Dr M. Majoor (Department of Otorhinolaryngology, Academisch Ziekenhuis, Utrecht, The Netherlands) for referring the patient described in cases 2 and 6, respectively.

References

1. Holliday RA, Reede DL. MRI of mastoid and middle ear disease. *Rad Clin North Am* 1989;27:283–299

2. Brogan M, Chakeres DW. Gd-DTPA-enhanced MR imaging of cochlear schwannoma. *AJNR* 1990;11:407–408
3. Seltzer S, Mark AS. Contrast enhancement of the labyrinth on MR scans in patients with sudden hearing loss and vertigo: evidence of labyrinthine disease. *AJNR* 1991;12:13–16
4. Brogan M, Chakeres DW, Schmalbrock P. High-resolution 3DFT-MR imaging of the endolymphatic duct and soft tissues of the otic capsule. *AJNR* 1991;12:1–11
5. Casselman JW, Kuhweide R., Deimling M, Ampe W, Dehaene I, Meeus L. Constructive interference in steady state (CISS)-3DFT MR imaging of the inner ear and cerebellopontine angle. *AJNR* 1993;14:47–57
6. Tanioka H, Shirakawa T, Machida T, Sasaki Y. Three dimensional reconstructed MR imaging of the inner ear. *Radiology* 1991;178: 141–144
7. Patz S. Some factors that influence the steady state in "steady state" free precession. *Magn Reson Imaging* 1988;6:405–413
8. Babin RW, Harker LA. Intralabyrinthine acoustic neurinomas. *Otolaryngol Head Neck Surg* 1980;88:455–461
9. Matthews VP, Kuharik MA, Edwards MK, D'Amour PG, Azzarelli B, Dreesen RG. Gd-DTPA-enhanced MR imaging of experimental bacterial meningitis: evaluation and comparison with CT. *AJNR* 1988;9:1045–1050
10. Brant-Zawadzki M, Berry I, Osaki L, et al. Gd-DTPA in clinical MR of the brain. I. Intraaxial lesions. *AJR* 1986;147:1223–1230
11. Lo WM. Tumors of the temporal bone and the cerebellopontine angle. In: Som PM, Bergeron RT, eds. *Head and neck imaging.* 2nd ed. St. Louis: Mosby, 1991:925–1115
12. Swartz JD. The otodystrophies. In: Swartz JD, ed. *Imaging of the temporal bone.* New York: Thieme, 1986:161–177
13. Swartz JD. Trauma and miscellaneous disorders. In: Som PM, Bergeron RT, eds. *Head and neck imaging.* 2nd ed. St. Louis: Mosby, 1991:1030–1046
14. Mafee MF, Charletta D, Kumar A, Belmont H. Large vestibular aqueduct and congenital sensorineural hearing loss. *AJNR* 1992;13:805–819
15. Jackler RK, De La Cruz A. The large vestibular aqueduct syndrome. *Laryngoscope* 1989;99:1238–1242
16. Levenson MJ, Parisier SC, Jacobs M, Edelstein DR. The large vestibular aqueduct syndrome in children. *Arch Otolaryngol Head Neck Surg* 1989;115:54–58
17. Fisher ER, Hellstrom HR. Cogan's syndrome and systemic vascular disease. *Arch Pathol* 1961;72:572–592
18. Wolff D, Bernhard WG, Tsutsumi S, Ross IS, Nussbaum HE. The pathology of Cogan's syndrome causing profound deafness. *Ann Otol Rhinol Laryngol* 1965;74:507–520